FERMILAB-PUB-12-038-T

# Sterile neutrinos and indirect dark matter searches in IceCube

Carlos A. Argüelles[1,2*] and Joachim Kopp[2†]

[1] *Sección Física, Departamento de Ciencias, Pontificia Universidad Católica del Perú, Apartado 1761, Lima, Peru and*

[2] *Fermilab, Theoretical Physics Department, PO Box 500, Batavia, IL 60510, USA*

(Dated: March 27, 2012)

If light sterile neutrinos exist and mix with the active neutrino flavors, this mixing will affect the propagation of high-energy neutrinos from dark matter annihilation in the Sun. In particular, new Mikheyev-Smirnov-Wolfenstein resonances can occur, leading to almost complete conversion of some active neutrino flavors into sterile states. We demonstrate how this can weaken IceCube limits on neutrino capture and annihilation in the Sun and how potential future conflicts between IceCube constraints and direct detection or collider data might be resolved by invoking sterile neutrinos. We also point out that, if the dark matter–nucleon scattering cross section and the allowed annihilation channels are precisely measured in direct detection and collider experiments in the future, IceCube can be used to constrain sterile neutrino models using neutrinos from the dark matter annihilation.

## I. INTRODUCTION

The hunt for dark matter is currently at a very exciting, but also somewhat confusing stage. Many unexpected experimental results that have been reported over the past few years can be interpreted in terms of dark matter, but all of them could have more mundane explanations, and moreover the dark matter interpretations of different experimental data sets do not fit together in many cases. For instance, the signals reported by CoGeNT [1, 2], DAMA [3, 4] and CRESST [5] appear to be in some tension with the null results from other direct detection experiment, in particular CDMS [6, 7] and XENON-100 [8] (see, however, [9, 10]). Moreover, the dark matter parameter regions favored by CoGeNT, DAMA and CRESST do not coincide under standard assumptions on the dark matter halo [11–16] (see, however, refs. [17–20]). Also, if the recently observed anomalies in the cosmic electron and positron spectra [21, 22]) are due to dark matter annihilation or decay, this would imply dark matter masses of order 1 TeV (see, for instance, [23]), whereas the CoGeNT, DAMA and CRESST hints would indicate dark matter masses of order 10 GeV. It is thus clear that many of the potential hints for dark matter must have other explanations, and this illustrates that a single experiment might never be able to unambiguously identify dark matter. Only matching detections by several different experiments would convince the community at large that dark matter has been observed. Fortunately, the toolbox for dark matter search is quite large: Direct detection experiments like CoGeNT, DAMA, CRESST, CDMS and XENON-100 search for dark matter recoils on atomic nuclei; collider searches at the Tevatron and the LHC aim to directly produce dark matter particles and detect them through missing energy signatures; indirect searches look for the annihilation or decay products of astrophysical dark matter. Among the possible messengers are electrons and positrons, anti-protons, gamma rays, and neutrinos.

A special role is played by searches for neutrinos from dark matter annihilation in the Sun,

*Electronic address: `c.arguelles@pucp.edu.pe`
†Electronic address: `jkopp@fnal.gov`

Operated by Fermi Research Alliance, LLC under Contract No. De-AC02-07CH11359 with the United States Department of Energy.

which are carried out by the Super-Kamiokande [24, 25] and IceCube [26, 27] collaborations. Even though these searches probe the products of dark matter annihilation, the expected event rates are usually determined by the dark matter capture rate in the Sun and thus by the dark matter–nucleus scattering cross section. Therefore, these searches, even though indirect, are sensitive to the same observables as direct detection experiments and can directly test any potential direct detection signal (provided that dark matter can annihilate and that its annihilation products include neutrinos). In particular, many astrophysical uncertainties, for instance those associated with the local dark matter density, affect the Super-Kamiokande and IceCube searches in the same way as the direct searches, making the comparison between those experiments quite robust with respect to astrophysics.

On the other hand, neutrinos from dark matter annihilation in the Sun are strongly affected by neutrino oscillation physics. In this paper, we will investigate how the oscillations pattern of high-energy neutrinos from dark matter annihilation in the Sun can be modified by the existence of sterile neutrinos. Our study is motivated by the results of the LSND [28] and MiniBooNE [29] experiments, as well as the reactor antineutrino anomaly [30–32], all of which can be interpreted as hints for the existence of sterile neutrinos with masses of order 1 eV [33–36]. (Note, however, that even models with two sterile neutrinos cannot resolve all tension in the global data set.) We will argue that, if sterile neutrinos exist, neutrinos from dark matter annihilation can encounter new Mikheyev-Smirnov-Wolfenstein (MSW) resonances when propagating out of the Sun, and that these resonances can potentially convert a large fraction of them into undetectable sterile states. This can weaken constraints on dark matter annihilation in the Sun significantly. (The existence of new MSW resonances in the presence of sterile neutrinos has also been investigated recently in the context of IceCube atmospheric neutrino data [37–41].) On the positive side, if the dark matter–nucleon scattering cross section and the dark matter annihilation channels are precisely determined elsewhere, for instance in direct detection and collider experiments, IceCube can be used as a sensitive tool for constraining sterile neutrino models.

The outline of the paper is as follows: In section II, we review the relevant aspects of the formalism of neutrino oscillations and discuss the effect of MSW resonances on the oscillation probabilities of high-energy neutrinos in the Sun. We then describe in section III how we compute the expected neutrino signal from dark matter annihilation in the IceCube detector, and in section IV we show how the existence of sterile neutrinos modifies the dark matter constraints from IceCube. We will discuss our results and conclude in section VI.

## II. NEUTRINO OSCILLATIONS AND NEUTRINO INTERACTIONS IN THE SUN

Neutrinos from dark matter annihilation in the Sun probe a very unique regime of neutrino oscillations: They are produced in a region of very high matter density ($\sim 150$ g/cm$^3$) at the center of the Sun [42], but with energies that can be much higher than those at which neutrino oscillations in the Sun are usually studied.

In the standard three-flavor oscillation framework, it is well known from the study of low-energy ($\mathcal{O}$(MeV)) solar neutrinos that strong transitions between electron neutrinos, $\nu_e$, and muon/tau neutrinos, $\nu_\mu$, $\nu_\tau$, take place in a region where the number density of electrons $N_e$ reaches a critical value, given by the Mikheyev-Smirnov-Wolfenstein (MSW) resonance condition [43–46]

$$N_e^{\rm low} = a_{\rm CP} \cos\theta_{12} \frac{\Delta m^2_{21}}{2E_\nu} \frac{1}{\sqrt{2}G_F} \,. \tag{1}$$

Here, $E_\nu$ is the neutrino energy, $G_F$ is the Fermi constant, $\theta_{12}$ and $\Delta m^2_{21}$ are the usual solar neutrino mixing parameters, and $a_{\rm CP} = 1$ $(-1)$ for neutrinos (antineutrinos). The MSW resonance

condition can be understood if we recall that according to the Fermi theory of weak interactions the local matter potential due to $W$ exchange with an electron, which is felt by electron-neutrinos but not by muon and tau neutrinos, is given by $\sqrt{2}a_{CP}G_F n_e(r)$, with $n_e(r) = \langle \bar{e}\gamma^0 e \rangle$ the electron number density at a distance $r$ from the center of the Sun. At high matter density near the center, the flavor-diagonal MSW potential is larger than the flavor-off-diagonal neutrino mass term $\Delta m^2_{21}/2E_\nu$ for multi-MeV neutrinos. Thus mixing between $\nu_e$ and $\nu_\mu$, $\nu_\tau$ is suppressed, and mass and flavor eigenstate almost coincide. For instance, the flavor eigenstate $\nu_e$ is almost equal to the mass eigenstate $\nu_2$ for multi-MeV neutrinos produced at the center of the Sun. At low matter density in the outer layers of the Sun, on the other hand, the mass terms dominate over the potential term, so that the effective mixing matrix is close to the vacuum mixing matrix, according to which $\nu_e$ is mostly composed of $\nu_1$. If the change in the matter density is not too fast, neutrinos cannot "jump" from one mass eigenstate to another, so that a neutrino produced as an almost pure $\nu_2$ will still be in an almost pure $\nu_2$ state when it exits the Sun. However, its flavor composition has changed dramatically, and in fact, the $\nu_e$ admixture to $\nu_2$ in vacuum is given $|U_{e2}|^2 \simeq \sin^2\theta_{12} \simeq 0.31$ (using the standard parameterization [46] and the current best fit values [47, 48] for the leptonic mixing matrix). Thus, almost 70% of the neutrinos are converted to $\nu_\mu$, $\nu_\tau$ on their way out of the Sun. The flavor-conversion happens predominantly at the transition between the matter potential-dominated and the mass mixing-dominated regime, where the two terms are of similar magnitude. This requirement leads precisely to the condition (1).

For energies above $\sim$ 100 MeV (not accessible with conventional solar neutrinos), a second MSW resonance appears at a higher density

$$N_e^{\rm high} = a_{\rm CP}\cos\theta_{13}\frac{\Delta m^2_{31}}{2E_\nu}\,\frac{1}{\sqrt{2}G_F}\,. \tag{2}$$

This second resonance leads to strong $\nu_e \leftrightarrow \nu_\mu, \nu_\tau$ transitions if $\Delta m^2_{31} > 0$, and to strong $\bar{\nu}_e \leftrightarrow \bar{\nu}_\mu, \bar{\nu}_\tau$ transitions for $\Delta m^2_{31} < 0$.

The requirement that the change in matter density be not too fast (see above) can be made more precise. One can show that resonant flavor transitions in the $(ij)$-sector cease when the *adiabaticity condition* [46]

$$\gamma_r \equiv \left(\frac{\Delta m^2_{ij}}{2E_\nu}\sin 2\theta_{ij}\right)^2 \frac{1}{|\dot{V}|_{\rm res}} \gg 1 \tag{3}$$

is no longer fulfilled. Here, $\gamma_r$ is called the adiabaticity parameter at the resonance and $|\dot{V}|_{\rm res}$ denotes the gradient of the MSW potential $V = \sqrt{2}G_F N_e$ at the location of the resonance. Loss of adiabaticity thus occurs for small mixing angles, small $\Delta m^2$ and high energies. In the case of the resonance in the (12)-sector, which turned out to be the solution to the long-standing solar neutrino problem, we expect adiabatic transitions below $\sim$ 10 GeV, and non-adiabatic behavior above. (Note that, if flavor transitions of solar neutrinos were non-adiabatic, an initial $\nu_e$ would leave the Sun not as a $\nu_2$ mass eigenstate, but as a superposition of the form $U^*_{e1}|\nu_1\rangle + U^*_{e2}e^{i\phi}|\nu_2\rangle$, with the oscillation phase $\phi$. After averaging over $\phi$, this would lead to a $\nu_e$ survival probability given by $1 - \frac{1}{2}\sin^2 2\theta_{12}$, in conflict with the experimental data on solar neutrinos.)

The neutrino oscillation probabilities in the Sun in the standard three-flavor framework are plotted as a function of energy in figures 1 and 2 (black lines). Note that in computing these oscillations probabilities, we treat the final neutrino flux as a completely incoherent mixture of mass eigenstates. This reflects the averaging of the oscillation probability over the size of the neutrino production region at the core of the Sun, the annual variation in the Earth–Sun distance and the experimental energy resolution. The transition between the adiabatic and non-adiabatic regimes is clearly visible in figures 1 and 2 at energies around 10 GeV. At typical solar neutrino

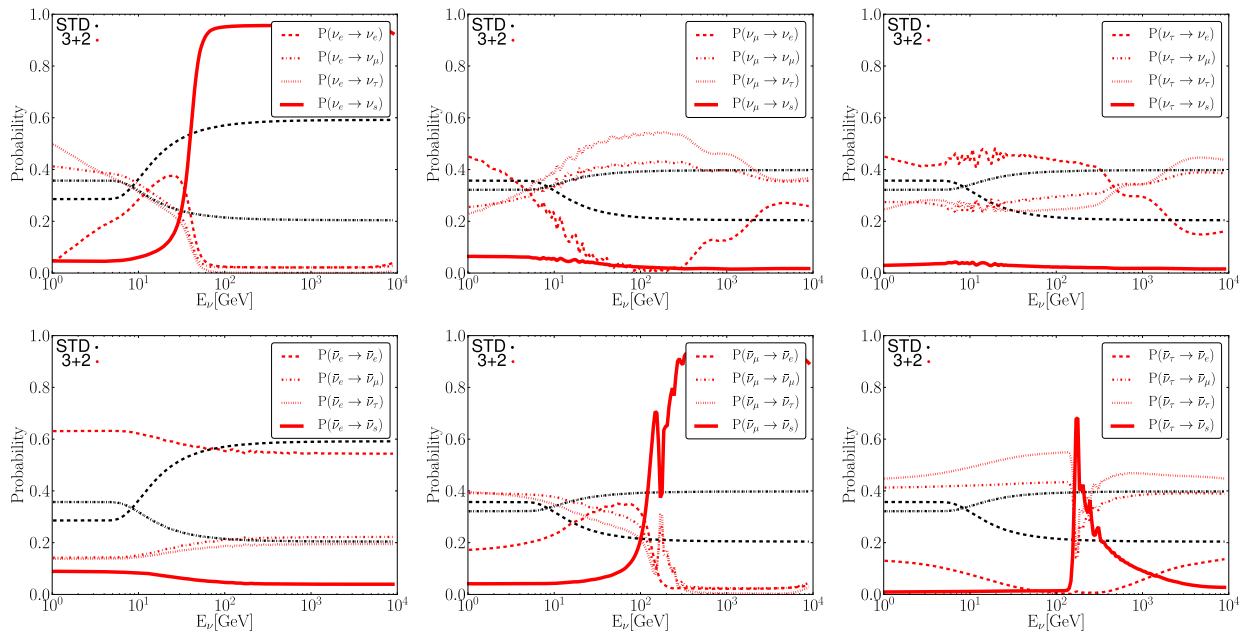


Figure 1: Flavor transition probabilities in the Sun as a function of energy for an initial $\nu_e$ (left), an initial $\nu_\mu$ (center), and an initial $\nu_\tau$ (right). We treat the final neutrino flux as a fully incoherent mixture of neutrino mass eigenstates. The top plots are for neutrinos, the ones at the bottom are for anti-neutrinos. Black lines are for standard three-flavor oscillation, whereas red lines are for a representative "$3+2$" model with two sterile neutrinos (see text for details). Absorption and $\tau$ regeneration effects are neglected in these plots. Note that the black dotted lines ($\nu_x \to \nu_\tau$ in the SM) and the black dot-dashed lines ($\nu_x \to \nu_\mu$ in the SM) lie on top of each other since $\nu_\mu$–$\nu_\tau$ mixing is assumed to be maximal.

energies of few MeV, the $\nu_e$ survival probability has the expected value of $\sin^2\theta_{12} \simeq 0.3$, while in the non-adiabatic regime, it is $1 - \frac{1}{2}\sin^2 2\theta_{12} \simeq 0.6$. (Small deviations from these values can arise from the inclusion of three-flavor effects, in particular a non-zero $\theta_{13}$.)

If sterile neutrinos exist, the oscillation phenomenology becomes much richer. Even if *vacuum* oscillations between active and sterile neutrino flavors are negligible because of small mixing angles, active–sterile oscillations *in matter* can be significant, in particular at the high energies relevant to neutrinos from dark matter annihilation. The $n$-flavor MSW potential has the form

$$V = (n_e - n_n/2, -n_n/2, -n_n/2, 0, \dots)\,, \tag{4}$$

where the terms containing the neutron density $n_n$ originate from coherent forward scattering through $Z^0$ exchange. These terms are usually neglected in the three-flavor framework since they are flavor-universal and therefore cannot contribute to oscillations among active neutrinos. However, they become relevant in the presence of sterile states. In particular, there will be additional MSW resonances whenever any of the matter potential terms becomes equal to any of the mass terms in the Hamiltonian. These MSW resonance can lead to nearly complete conversion of certain neutrino (or antineutrino) flavors into sterile states on the way out of the Sun.

To illustrate this observation, which is the main topic of this paper, we consider a sterile neutrino scenario similar to the one that has been shown in Refs. [33, 36] to provide a reasonably good fit to the global neutrino data, including the anomalous LSND and MiniBooNE results. The model has

two sterile neutrino flavors $\nu_{s1}$, $\nu_{s2}$ and two new mass eigenstates $\nu_4$, $\nu_5$ with mixing parameters

$$\begin{gathered}
\sin^2\theta_{12} = 0.32 \qquad \sin^2 2\theta_{13} = 3\times 10^{-3} \qquad \sin^2\theta_{23} = 0.45 \\
\Delta m^2_{21} = 7.6\times 10^{-5}\ \mathrm{eV}^2 \qquad \Delta m^2_{31} = 2.38\times 10^{-3}\ \mathrm{eV}^2 \\
\Delta m^2_{41} = 0.47\ \mathrm{eV}^2 \qquad \Delta m^2_{51} = 0.90\ \mathrm{eV}^2 \\
\sin^2 2\theta_{14} = 0.060 \\
\sin^2 2\theta_{24} = 0.055 \qquad \sin^2 2\theta_{34} = 0.000 \qquad \sin^2 2\theta_{15} = 0.086 \\
\sin^2 2\theta_{25} = 0.088 \qquad \sin^2 2\theta_{35} = 0.002 \qquad \delta_{13} = 1.47\pi \qquad \delta_{14} = 0.77\pi \qquad \delta_{15} = 1.086\pi
\end{gathered} \tag{5}$$

Here, we use the parameterization

$$U_{3+2} = R_{45}R_{35}R_{25}R^{\delta}_{15}R_{34}R_{24}R^{\delta}_{14}R_{23}R^{\delta}_{13}R_{12} \tag{6}$$

for the leptonic mixing matrix, where $R_{ij}$ denotes a rotation matrix in the $(ij)$ plane with rotation angle $\theta_{ij}$, and $R^{\delta}_{ij}$ denotes a similar rotation matrix which in addition carries a complex phase $\delta_{ij}$:

$$R_{ij} = \begin{pmatrix} \ddots & & & & \\ & \cos\theta_{ij} & \cdots & \sin\theta_{ij} & \\ & \vdots & & \vdots & \\ & -\sin\theta_{ij} & \cdots & \cos\theta_{ij} & \\ & & & & \ddots \end{pmatrix}, \qquad R^{\delta}_{ij} = \begin{pmatrix} \ddots & & & & \\ & \cos\theta_{ij} & \cdots & \sin\theta_{ij}e^{-i\delta_{ij}} & \\ & \vdots & & \vdots & \\ & -\sin\theta_{ij}e^{i\delta_{ij}} & \cdots & \cos\theta_{ij} & \\ & & & & \ddots \end{pmatrix}. \tag{7}$$

In a "$3+2$" scenario like equation (5), the new MSW resonances converting active neutrinos into sterile ones affect antineutrinos more strongly than neutrinos, but since neutrino cross sections are larger than antineutrino cross sections, we expect the impact of sterile neutrinos on dark matter searches to be only moderate, especially in detectors like IceCube and Super-Kamiokande which cannot distinguish neutrinos from antineutrinos. (Below, we will also discuss a $3+3$ toy model in which effects are larger.)

The neutrino oscillation probabilities in the Sun for this sterile neutrino scenario are shown in figure 1 as red curves. The most striking feature is the strong conversion of $\bar{\nu}_\mu$ (and to some degree also $\bar{\nu}_\tau$) into sterile neutrinos at energies above $\sim 200$ GeV. Indeed, we can see from equation 1 (with the replacements $\theta_{12} \to \theta_{14} \simeq 0$, $\Delta m^2_{21} \to \Delta m^2_{41} \simeq -1$ eV$^2$, and $N_e \to -N_n/2$) that above $E_\nu \sim 100$ GeV, the MSW resonance between active and sterile neutrinos lies within the Sun. Therefore, high energy $\bar{\nu}_\mu$ and $\bar{\nu}_\tau$ produced from dark matter annihilation at the center of the Sun will be almost fully converted into sterile neutrinos, leaving as detectable states only neutrinos, and antineutrinos from the $\bar{\nu}_e$ component of the primary flux. For a given dark matter mass, annihilation channel and annihilation cross section, the expected event number in a neutrino detector is thus reduced, so that experimental constraints on dark matter annihilation in the Sun become weaker.

In addition to the $3+2$ scenario, we are also going to consider a $3+3$ toy model with 3 sterile neutrinos. The oscillation parameters in this model are chosen such that each active neutrino flavor eigenstate mixes with only one of the sterile neutrinos. This can be achieved by choosing mass squared difference $\Delta m^2_s \equiv \Delta m^2_{41} \simeq \Delta m^2_{52} \simeq \Delta m^2_{63}$ and mixing angles $\theta_s \equiv \theta_{14} \simeq \theta_{25} \simeq \theta_{36}$ (all other active–sterile mixing angles are zero), so that the sterile neutrino sector is a mirror image of the active neutrino sector as far as vacuum oscillations are concerned. (Similar models have been considered in [49].) The parameterization of the leptonic mixing matrix is here

$$U_{3+3} = R_{36}R_{25}R_{14}R_{23}R^{\delta}_{13}R_{12} \tag{8}$$

Unless specified otherwise, we choose $\Delta m^2_{41} = 0.1$ eV$^2$ and $\sin^2 2\theta_s = 0.03$. In general, if $\Delta m^2_{41}$, $\Delta m^2_{52}$, $\Delta m^2_{63} \gg \Delta m^2_{21}$, $|\Delta m^2_{31}|$, conversions of active neutrinos into sterile neutrinos can be understood in a simple two-flavor framework as long as the distance travelled by the neutrinos is much shorter than the active neutrino oscillation lengths $L^{\rm osc}_{21} = 4\pi E_\nu/\Delta m^2_{21}$ and $L^{\rm osc}_{31} = 4\pi E_\nu/|\Delta m^2_{31}|$. This remains true even in matter. In this case, the effective two-flavor oscillations between an active flavor and its corresponding sterile flavor are affected by an MSW resonance. The resonance conditions are, in analogy to equations (1) and (2):

$$N_e = a_{\rm CP} \cos\theta_{14} \frac{\Delta m^2_{41}}{2E_\nu} \frac{1}{\sqrt{2}G_F}\,, \qquad (\nu_e \leftrightarrow \nu_{s1} \text{ transitions}) \tag{9}$$

$$-\frac{N_n}{2} = a_{\rm CP} \cos\theta_{25} \frac{\Delta m^2_{52}}{2E_\nu} \frac{1}{\sqrt{2}G_F}\,, \qquad (\nu_\mu \leftrightarrow \nu_{s2} \text{ transitions}) \tag{10}$$

$$-\frac{N_n}{2} = a_{\rm CP} \cos\theta_{36} \frac{\Delta m^2_{63}}{2E_\nu} \frac{1}{\sqrt{2}G_F}\,. \qquad (\nu_\tau \leftrightarrow \nu_{s3} \text{ transitions}) \tag{11}$$

We see from these equations that the resonance between $\nu_e$ and the first sterile flavor eigenstate $\nu_{s1}$ will be in the neutrino sector ($a_{\rm CP} = 1$), whereas the $\nu_\mu \leftrightarrow \nu_{s2}$ and $\nu_\tau \leftrightarrow \nu_{s3}$ resonances affect antineutrinos ($a_{\rm CP} = -1$). This behavior is reflected in figure 2, where we show the flavor transition probabilities for all oscillation channels in the $3+3$ model as a function of energy. We see that in a large energy range $\nu_e$, $\bar\nu_\mu$ and $\bar\nu_\tau$ are almost fully converted into sterile states. We expect that this will lead to a considerable weakening of the limits IceCube can set on dark matter capture and annihilation in the Sun.

Note that this weakening could be even more pronounced if the mostly active neutrino mass eigenstates were *heavier* than the mostly sterile ones, since in that case the MSW resonances for second and third generation neutrinos would move from the antineutrino sector to the neutrino sector, which is more important for IceCube's dark matter search because neutrino interaction cross sections are about a factor of 3 larger than antineutrino cross sections. We do not consider this possibility here since relatively heavy active neutrinos would be in potential conflict with cosmology [50–53]. (These conflict can potentially be avoided in non-minimal cosmologies [52, 53] and in models where the relic abundance of sterile neutrinos is reduced, see for instance references [54, 55] for a discussion of such models.)

Apart from oscillation, the propagation of high-energy neutrinos through the Sun is also affected by non-coherent neutral current (CC) and charged current (CC) interactions. NC interactions change the neutrino energy, whereas CC interactions lead to absorption and possible reemission of neutrinos in the decay of secondary $\mu$ or $\tau$ leptons. Since secondary muons are usually thermalized before they decay, reemission of *high-energy* neutrinos is only possible in the case of $\nu_\tau + X \to \tau + X'$ CC interactions ("$\tau$ regeneration"). In figure 3 we plot the non-interaction ("survival") probability $P_{\rm survival}$ for neutrinos from dark matter annihilation on their way out of the Sun as a function of the neutrino energy. $P_{\rm survival}$ can be calculated as

$$P_{\rm survival}(E_\nu) = \exp\left[ -\int dx\, \rho(x) \left( \sigma_{{\rm CC}_e} p_e(x) + \sigma_{{\rm CC}_\mu} p_\mu(x) + \sigma_{{\rm CC}_\tau} p_\tau(x) + \sigma_{\rm NC} p_{\rm active}(x) \right) \right], \tag{12}$$

where $p_\alpha(x)$ is the probability of the neutrino being in the flavor state $\alpha$ at position $x$, $p_{\rm active}(x) \equiv \sum_{\alpha=e,\mu,\tau} p_\alpha(x)$, and the integral runs over the neutrino trajetory,

## III. SIMULATION TECHNIQUES

To estimate quantitatively how existing limits on dark matter annihilation in the Sun are modified in the presence of sterile neutrinos, we have carried out numerical simulations. We

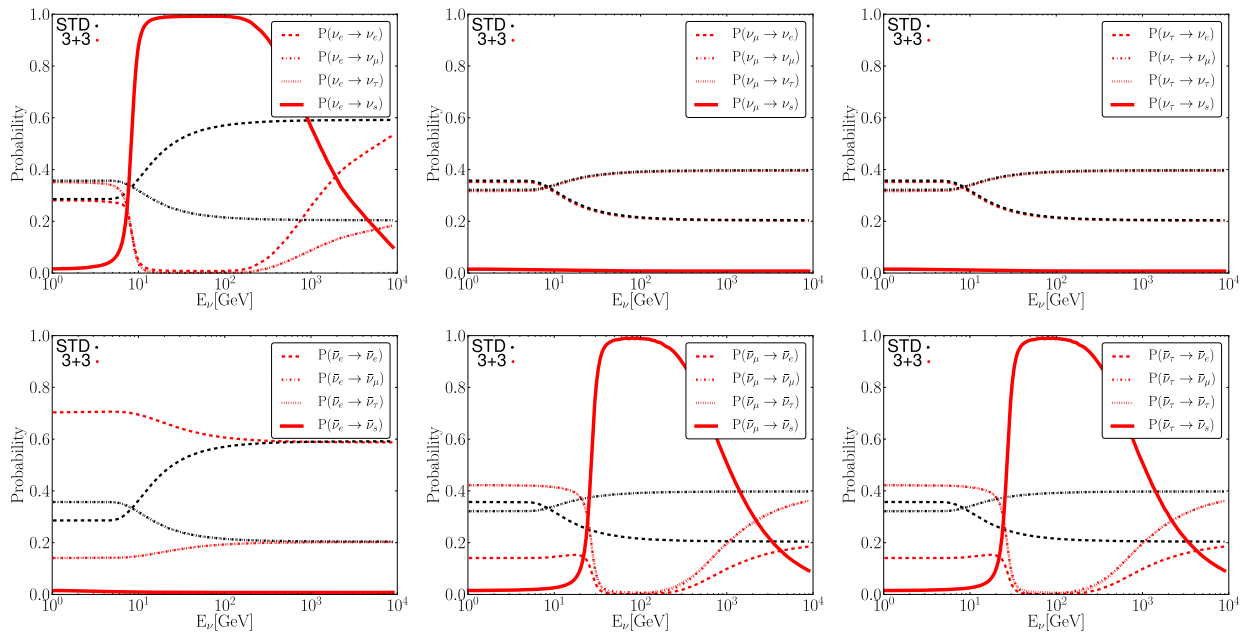


Figure 2: Flavor transition probabilities in the Sun as a function of energy for an initial $\nu_e$ (left), an initial $\nu_\mu$ (center), and an initial $\nu_\tau$ (right). We treat the final neutrino flux as a fully incoherent mixture of neutrino mass eigenstates. The top plots are for neutrinos, the ones at the bottom are for anti-neutrinos. Black lines are for standard three-flavor oscillation, whereas red lines are for a "$3+3$" toy model with three sterile neutrinos (see text for details). Absorption and $\tau$ regeneration effects are neglected in these plots. Note that the black dotted lines ($\nu_x \to \nu_\tau$ in the SM) and the black dot-dashed lines ($\nu_x \to \nu_\mu$ in the SM) lie on top of each other since $\nu_\mu$–$\nu_\tau$ mixing is assumed to be maximal.

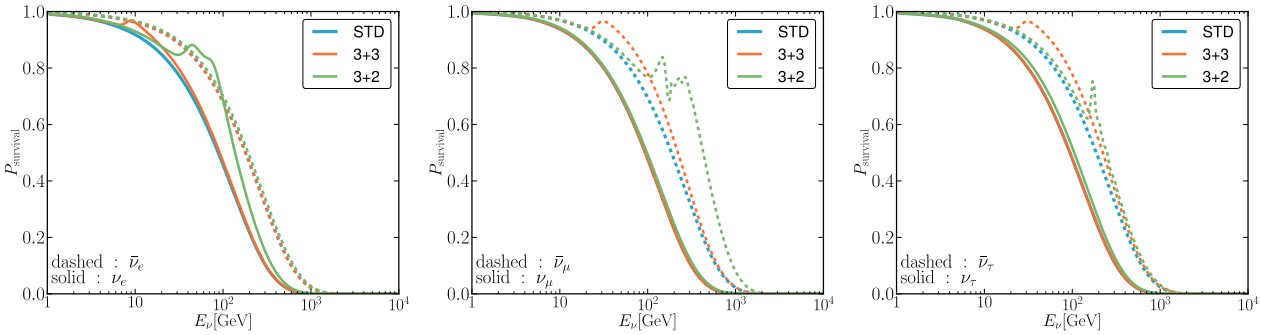


Figure 3: Survival (= non-interaction) probabilities for high-energy neutrinos from dark matter annihilation on their way out of the Sun. This plot shows only the effect of neutrino absorption or scattering, not that of flavor transitions. Flavor transitions do, however, affect the absorption probability indirectly: for instance a neutrino that has been converted into a sterile flavor can no longer be absorbed. We show results here for standard three-flavor oscillations, for the best fitting $3+2$ model, and for a $3+3$ toy model. The features in the $3+2$ and $3+3$ curves are due to the interplay of active–sterile conversion and active neutrino interactions.

compute the dark matter capture rate as a function of the dark matter mass and scattering cross section using the formulae from [56] and assuming a local WIMP density of 0.3 GeV/cm$^3$ with an isothermal velocity distribution and velocity dispersion 220 km/sec. We assume the annihilation cross section to be large enough for the capture and annihilation reactions to be in equilibrium, so that the annihilation rate is equal to half the capture rate. We use initial neutrino spectra from [57], which were generated using `WimpSim` [58].

To propagate the neutrinos out of the Sun, we use our own Monte Carlo code, which is capable of working with an arbitrary number of neutrino flavors $n$, and simulates $n$-flavor oscillations in matter as well as NC and CC neutrino scattering in the Sun, including $\tau$ regeneration. We use the `nusigma` package [57, 58] to calculate the neutrino cross sections, and TAUOLA [59] for decaying secondary $\tau$'s.

In practice, we proceed as follows: We propagate the $n$-component neutrino state vector $\psi(t)$ out of the Sun using the `rkf45` Runge-Kutta-Fehlberg algorithm from the GNU Scientific Library [60] to solve the evolution equation

$$i\frac{d}{dt}\psi(t) = \frac{1}{2E_\nu}U\begin{pmatrix} 0 & & & & \\ & \Delta m^2_{21} & & & \\ & & \Delta m^2_{31} & & \\ & & & \Delta m^2_{41} & \\ & & & & \ddots \end{pmatrix} U^\dagger\psi(t) + \sqrt{2}G_F\begin{pmatrix} N_e(t) - \frac{N_n(t)}{2} & & & & \\ & -\frac{N_n(t)}{2} & & & \\ & & -\frac{N_n(t)}{2} & & \\ & & & 0 & \\ & & & & \ddots \end{pmatrix}\psi(t)\,. \tag{13}$$

After each Runge-Kutta step, we determine randomly if the neutrino undergoes an incoherent interactions during that step. The probability for a CC or NC interaction is given by $P_{\mathrm{CC/NC}} = \sigma_{\mathrm{CC/NC}}/(\sigma_{\mathrm{CC}}+\sigma_{\mathrm{NC}}) \times \left[1-\exp\left(-\Delta r\, n(r)\,(\sigma_{\mathrm{CC}}+\sigma_{\mathrm{NC}})\right)\right]$, where $n(r)$ is the local nucleon number density, $\sigma_{\mathrm{CC(NC)}}$ is the charged current (neutral current) neutrino–nucleon scattering cross section, and $\Delta r$ is the current Runge-Kutta step size. If it is determined that the neutrino interacts through a neutral current, its energy after the interaction is picked randomly from the final state energy spectrum calculated using `nusigma` [57, 58]. Since we are treating neutrino propagation as a one-dimensional problem, we assume that the direction of travel does not change, and we continue to propagate the neutrino radially outward. In the case of a $\nu_e$ or $\nu_\mu$ charged current interactions, we simply discard the neutrino. In a charged current $\nu_\tau$ interactions, the original neutrino is also absorbed, but since the secondary $\tau$ lepton (unlike a secondary muon from a $\nu_\mu$ interaction) decays before it is stopped in matter, new high-energy neutrinos can be produced from its decay ("$\tau$ regeneration"). We use `TAUOLA` [59] to simulate $\tau$ decay, and propagate all secondary high-energy neutrinos out of the Sun individually.

We compute the expected event rate in the IceCube detector by multiplying the differential muon neutrino and antineutrino fluxes at the Earth the effective detector area $A_{\mathrm{eff}}(E_\nu)$ [61] and then integrating over energy. Note that we treat the neutrinos arriving at the Earth as a completely incoherent mixture of mass eigenstates (see section II). We have checked that neutrino absorption in the Earth ("Earth shadowing" [62, 63]) is negligible for our results. We also do not need to consider oscillations in the Earth, which are only relevant for neutrino energies close to one of the terrestrial MSW resonance. However, the two standard resonances driven by $\Delta m^2_{21}$ and $\Delta m^2_{31}$ are relevant only at neutrino energies below the IceCube energy threshold, whereas the resonances mixing active neutrino and eV-scale sterile neutrinos affect only $\mathcal{O}$(TeV) neutrinos, which cannot even leave the Sun efficiently (see figure 3). Note that the effective area given in [61] has been computed from a simulation of the full 86-string IceCube detector, whereas the latest published dark matter limits from IceCube are based on data taken in the 40-string IceCube configuration and in the older AMANDA-II detector. Since we will ultimately use our simulation only to compute

*ratios* of event rates between different oscillation models, we expect the systematic bias introduced that way to be small. Note also that $A_{\rm eff}(E_\nu)$ as given in [61] is the combined effective area for neutrinos and antineutrinos. Since in sterile neutrino models, the relative importance of neutrinos and antineutrinos in the IceCube signal changes, we need seperate effective areas for neutrinos ($A^\nu_{\rm eff}(E_\nu)$) and antineutrinos ($A^{\bar\nu}_{\rm eff}(E_\nu)$). We obtain them according to

$$A^\nu_{\rm eff}(E_\nu) = A_{\rm eff}(E_\nu)\frac{\sigma^\nu_{\rm CC}(E_\nu)\, d_{\mu^-}(E_\mu)}{\sigma^\nu_{\rm CC}(E_\nu)\, d_{\mu^-}(E_\mu) + \sigma^{\bar\nu}_{\rm CC}(E_\nu)\, d_{\mu^+}(E_\mu)}\,, \tag{14}$$

$$A^{\bar\nu}_{\rm eff}(E_\nu) = A_{\rm eff}(E_\nu)\frac{\sigma^{\bar\nu}_{\rm CC}(E_\nu)\, d_{\mu^+}(E_\mu)}{\sigma^\nu_{\rm CC}(E_\nu)\, d_{\mu^-}(E_\mu) + \sigma^{\bar\nu}_{\rm CC}(E_\nu)\, d_{\mu^+}(E_\mu)}\,, \tag{15}$$

with the charged current neutrino–nucleon (antineutrino–nucleon) cross section $\sigma^\nu_{\rm CC}(E_\nu)$ ($\sigma^{\bar\nu}_{\rm CC}(E_\nu)$), and the muon (antimuon) range $d_{\mu^-}(E_\mu)$ ($d_{\mu^+}(E_\mu)$). For simplicity, we assume a one-to-one relation between the neutrino energy $E_\nu$ and the secondary muon energy $E_\mu$: $E_\mu = (1 - y_{\rm CC}(E_\nu))E_\nu$, where $y_{\rm CC}$ is the mean charged current inelasticity parameter [64]. We have checked that using full differential cross sections would not significantly change our results.

We have verified our Monte Carlo code by comparing its predictions to published results from [57, 58, 65, 66].

While the advantage of the Monte Carlo technique is certainly its flexibility, it is also quite computationally intensive. Since we are also interested in carrying out parameter scans over different sets of sterile neutrino parameters (see section V below), we have also developed a faster code, which does not take into account $\tau$ regeneration and energy loss in neutral current interactions. Instead, it simply considers all neutrinos that interact in the Sun in any way (NC or CC) to be lost to detection. Thus, for each given set of oscillation parameters and for each neutrino energy, we need to solve the equation of motion only once to determine the oscillation probabilities for those neutrinos which do not interact. At each Runge-Kutta step, we also keep track of the interaction probability to obtain simultaneously the fraction of neutrinos at the considered energy which leave the Sun without interacting.

We compare the results of our full Monte Carlo simulation to those of the simplified method in figure 4. We also show the flux of secondary neutrinos from $\tau$ regeneration, and we notice that these neutrinos account for most of the difference between the MC results and the ones from the simplified method. (Another small contribution to this difference comes from neutrinos that have undergone NC scattering, but are still within the accessible energy range.) This conclusion is the same for standard three-flavor oscillations (black and gray curves in figure 4) and for the $3 + 3$ model (red curves).

## IV. MODIFIED ICECUBE LIMITS ON DARK MATTER CAPTURE IN THE SUN

In figure 5 we show how the IceCube limits on spin-dependent dark matter–proton scattering need to be modified if sterile neutrinos exist (black and gray lines). For comparison we also show as colored lines limits from a number of direct dark matter searches. We have chosen the case of spin-dependent dark matter scattering here rather than the more common spin-independent interactions since the power of the IceCube limits compared to direct searches is greater in this case [27]. We expect the corrections to the IceCube limits due to sterile neutrinos to be very similar in the two cases, though.

Solid black lines in figure 5 are the published IceCube limits from [27, 61]; Dashed and dotted lines show the constraint obtained in the $3 + 2$ model and the $3 + 3$ toy model introduced in section II, respectively. To obtain these results, we have used the methods described in section III to predict the ratio of the event rates at IceCube with and without sterile neutrinos, and we have

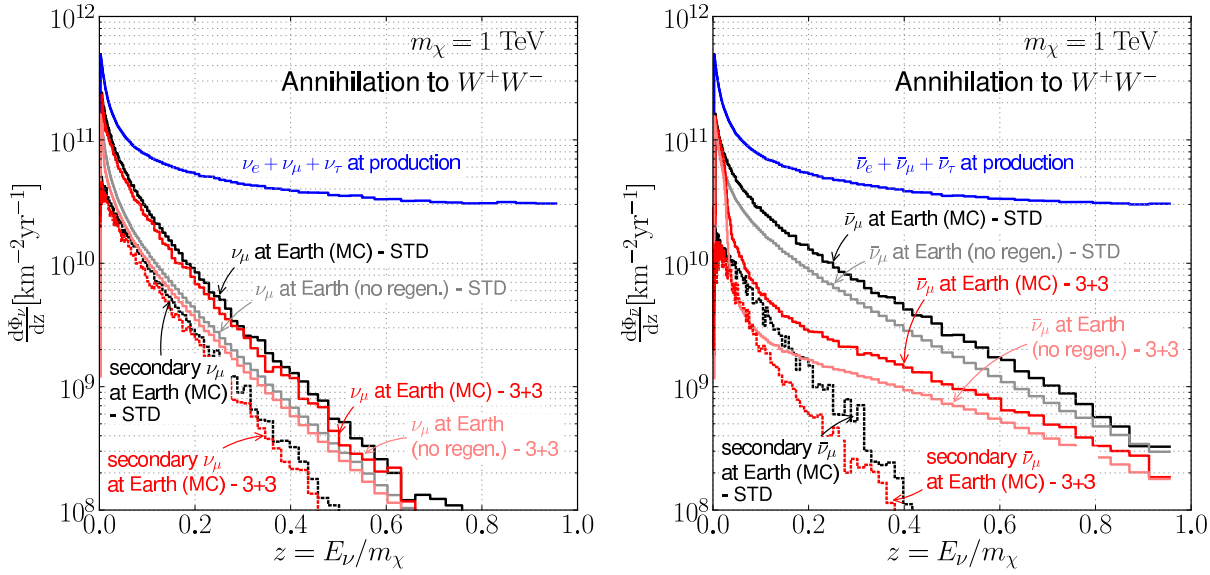


Figure 4: Predicted neutrino fluxes (left) and antineutrino fluxes (right) for annihilation of a 1 TeV WIMP into $W^+W^-$ in the Sun. We show the total neutrino flux at production, as well as the muon neutrino flux at the Earth. For illustration, we also show the flux of secondary neutrinos from $\tau$ regeneration, as well as the flux obtained using the simplified calculation that neglects regeneration and partial energy loss (see text for details). Results for standard oscillations ("STD") are shown in black, results for the $3+3$ toy model introduced in section II are shown in red.

then rescaled the published IceCube 90% CL limit on the dark matter–nucleon scattering cross section $\sigma_{90,\mathrm{STD}}$ (which was computed assuming standard oscillations) by this ratio. Specifically, if we denote the IceCube event rate by $N_{\mathrm{STD}}$, $N_{3+2}$ and $N_{3+3}$ for the standard oscillation, $3+2$, and $3+3$ scenarios, respectively, we compute the cross section limits in the $3+2$ and $3+3$ scenarios, $\sigma_{90,3+2}$ and $\sigma_{90,3+3}$, according to

$$\sigma_{90,3+2} = \sigma_{90,\mathrm{STD}} \frac{N_{3+2}}{N_{\mathrm{STD}}} \,, \tag{16}$$

$$\sigma_{90,3+3} = \sigma_{90,\mathrm{STD}} \frac{N_{3+3}}{N_{\mathrm{STD}}} \,. \tag{17}$$

We see that the $3+2$ model leads to a moderate weakening of the cross section limit, which can be understood from the fact that only electron neutrinos $\nu_e$ and muon antineutrinos $\bar{\nu}_\mu$ are substantially transformed into sterile states (see figure 1), and that these transitions happen only for neutrinos with energies above several hundred GeV, whose contribution to the muon flux at IceCube is suppressed due to the large absorption probability in the Sun. In the $3+3$ toy model, on the other hand, resonant flavor transitions happen already at lower energy (see figure 2), and they happen for $\nu_e$, $\bar{\nu}_\mu$ and $\bar{\nu}_\tau$.

As mentioned in section II, the effect could be even stronger if $\Delta m^2_{41}$, $\Delta m^2_{51}$, and $\Delta m^2_{61}$ were negative (which might, however, require non-standard cosmology to be consistent).

## V. DEPENDENCE ON STERILE NEUTRINO PARAMETERS

In section IV we have illustrated using two exemplary models how neutrino limits on dark matter capture and annihilation in the Sun are modified by oscillations into sterile neutrinos . We

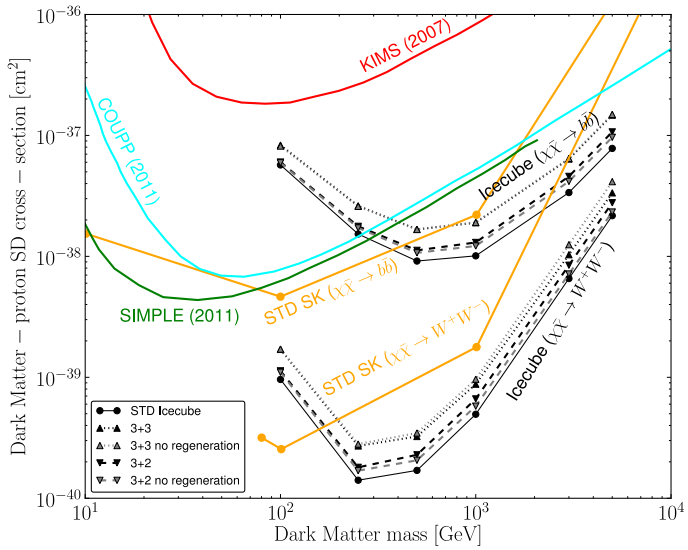


Figure 5: IceCube limits on spin-dependent dark matter-proton scattering [27, 61] in scenarios with sterile neutrinos (black/gray dashed and dotted lines) and in the standard oscillation ("STD") framework (black/gray solid lines) compared to data from direct detection experiments [24, 67–69] and from Super-Kamiokande (SK) [25] (colored lines). Black lines correspond to results based on our Monte Carlo (MC) code, whereas gray lines are based on a simplified calculation which does not include secondary neutrinos (see text for details). We see that for the $3+2$ scenario which provides the best fit to short baseline neutrino oscillation data, the limits are only moderately weakened. Our $3+3$ toy model, on the other hand, illustrates that larger modifications are possible.

are now going to study more systematically how the worsening of these limits depends on the sterile neutrino parameters. We do this using the $3+3$ toy model introduced in section II since this model has only two new parameters ($\theta_s$ and $\Delta m_s^2$), but still covers the most important phenomenological aspects of more general sterile neutrino scenarios.

We show in figure 6 the factor by which the IceCube limits on the spin-dependent dark matter–nucleon scattering cross section are weakened for a wide range of $\sin^2 2\theta_s$ and $\Delta m_s^2$ values. The shape of the contours can be understood as follows: At very large $\Delta m_s^2$, the new MSW resonances, equations (9)–(11) lie at a very high neutrino energy. For instance, at $\Delta m_s^2 = 1$ eV$^2$, equation (9) yields a resonance energy of about 60 GeV at solar core densities, i.e. only neutrinos with $E_\nu \gtrsim$ 60 GeV are affected by the resonance. Since very high energy neutrinos are mostly absorbed in the Sun, they do not contribute significantly to the IceCube limits. For somewhat lower $\Delta m_s^2$, the resonances move down in energy into the region relevant to IceCube. For too low $\Delta m_s^2$ or for too small $\theta_s$, on the other hand, MSW-enhanced flavor transitions become non-adiabatic (see equation (3) and related discussion), suppressing active–sterile transitions again. This happens first at high energy, which is why at low $\Delta m_s^2$ the correction factors shown in figure 6 are generally larger for dark matter annihilation into the soft $\bar{b}b$ channel than for annihilation in to the hard $W^+W^-$ final state.

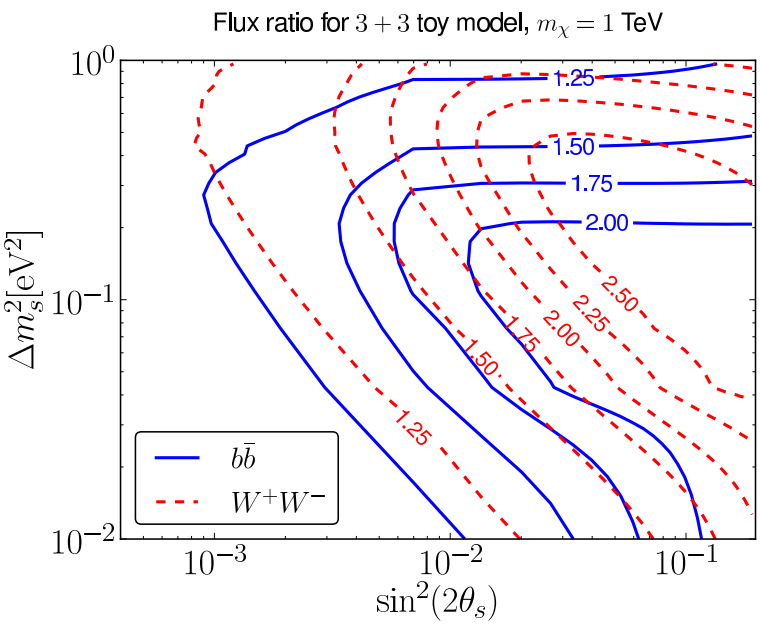


Figure 6: Weakening of IceCube limits on dark matter capture and annihilation in the Sun due to sterile neutrinos, assuming for illustrative purposes the $3+3$ toy model introduced in section II. The contours show the factor by which the IceCube limit on spin-dependent dark matter–proton scattering cross section for a 1 TeV WIMP. Red dashed contours are for annihilation into $W^+W^-$ (which yields a rather hard neutrino spectrum), blue solid contours are for annihilation into $\bar{b}b$ (which yields a much softer spectrum). At large $\Delta m_s^2$, oscillations into sterile neutrinos become less relevant because the active–sterile MSW resonances move to very high energies; at small $\Delta m_s^2$ or small $\sin^2 2\theta_s$, the MSW transitions become non-adiabatic.

## VI. DISCUSSION AND CONCLUSIONS

In this paper, we have shown how IceCube limits on dark matter capture and annihilation in the Sun are modified if eV-scale sterile neutrinos exist, as suggested by part of the short baseline oscillation data. Since IceCube is looking for high-energy neutrinos from dark matter annihilation in the center of the Sun, its results depend strongly on the oscillations of these neutrinos on their way out of the Sun. We have argued that in sterile neutrino scenarios new high-energy MSW resonances can lead to almost complete conversion of certain neutrino flavors into sterile states inside the Sun. In this case IceCube's constraints on dark matter–nucleon scattering can be significantly weakened, by a factor of two or more.

This may have interesting implications if in the future dark matter is detected in a direct search or at the LHC, but the parameters determined there are in conflict with limits (or signals) from neutrino telescopes. If the allowed dark matter annihilation channels and branching fractions are established at the LHC, such a conflict could then provide a clear and strong hint for the existence of sterile neutrinos. With sufficient data, neutrino telescopes would even be able to contribute the determination of the active–sterile mixing parameters.

*Note added:* While we were completing this work, reference [70] appeared on the arXiv, addressing similar topics.

**Acknowledgments**

It is a pleasure to thank Matthias Danninger for very useful discussions on the IceCube dark matter search. We are also grateful to the Dirección de Informática Académica at the Pontificia Universidad Católica del Perú (PUCP) for providing distributed computing support through the LEGION system. CA would like to thank Fermilab for warm hospitality and for support through the Latin American Students Program during his six month visit in summer 2011. CA is supported by the Dirección de Gestión de la Investigación at PUCP through grant DGI-2011-0180. Fermilab is operated by Fermi Research Alliance, LLC, under contract DE-AC02-07CH11359 with the United States Department of Energy.

## Appendix A: NUMERICS OF NEUTRINO OSCILLATION PROBABILITIES

In this appendix, we discuss the algorithm used to compute the neutrino oscillation probabilities in the Sun. As mentioned in section III we use an implementation of the well known Runge-Kutta (RK) algorithm [71], namely the `rkf45` algorithm implemented in the GNU Scientific Library [60]. In each iteration this algorithm uses a step function to evolve the neutrino state vector from a time $t_0$ to a time $t_0 + \Delta t$ by approximately solving the Schrödinger equation, where $\Delta t$ is chosen such that the optimal balance between speed and accuracy is achieved. Rather than working entirely in one basis, we transform the Schrödinger equation to an instantaneous interaction basis before each step. This instantaneous interaction basis is defined by the transformation

$$\psi_I(t;t_0) = S(t,t_0)\,\psi(t) \equiv e^{iH_0(t-t_0)}\psi(t)\,, \tag{A1}$$

where the Hamiltonian has been separated in the following manner

$$H(t) = H(t_0) + \Delta H(t;t_0)\,, \tag{A2}$$

with

$$H_0(t_0) = \frac{1}{2E_\nu} U D U^\dagger + V(t_0)\,, \qquad \Delta H(t;t_0) = V(t) - V(t_0)\,. \tag{A3}$$

Here $V(t)$ is the neutrino matter potential (see equation (4)), $E_\nu$ the neutrino energy, $U$ the leptonic mixing matrix, and $D = \mathrm{diag}(0, \Delta m^2_{21}, \Delta m^2_{31}, ...)$.

The Schrödinger equation in the interaction basis is

$$i\frac{d\psi_I}{dt} = H_I \psi_I \tag{A4}$$

with $H_I(t;t_0) = S(t,t_0)\,\Delta H\, S^\dagger(t,t_0)$. Since the matter potential changes slowly in the Sun and thus $H_I$ is small, the RK algorithm can choose a larger step size $\Delta t$ compared to a calculation in the flavor basis. Note that the elements $S_{jk}$ of the transformation matrix $S(t,t_0)$ can be evaluated efficiently by computing $\tilde{V}_{jm} e^{-i\lambda_m(t-t_0)} (\tilde{V}^\dagger)_{mk}$, where $\lambda_m$ are the eigenvalues of $H_0$, and $\tilde{V}$ is the matrix of the corresponding eigenvectors. After the evolution of the step has concluded we transform $\psi_I$ back to the flavor basis,

$$\psi(t_0 + \Delta t) = e^{-iH_0(t_0)\,\Delta t}\psi_I(t_0 + \Delta t)\,, \tag{A5}$$

and proceed to the next step, setting $t_0 \to t_0 + \Delta t$.

[1] C. Aalseth *et al.* (CoGeNT collaboration), Phys.Rev.Lett., **106**, 131301 (2011), `arXiv:1002.4703[astro-ph.CO]` .

[2] C. Aalseth, P. Barbeau, J. Colaresi, J. Collar, J. Diaz Leon, *et al.*, Phys.Rev.Lett., **107**, 141301 (2011), arXiv:1106.0650[astro-ph.CO] .
[3] R. Bernabei *et al.* (DAMA), Eur. Phys. J., **C56**, 333 (2008), arXiv:0804.2741[astro-ph] .
[4] R. Bernabei, P. Belli, F. Cappella, R. Cerulli, C. Dai, *et al.*, Eur.Phys.J., **C67**, 39 (2010), arXiv:arXiv:1002.1028[astro-ph.GA] .
[5] G. Angloher, M. Bauer, I. Bavykina, A. Bento, C. Bucci, *et al.*, (2011), arXiv:1109.0702[astro-ph.CO] .
[6] Z. Ahmed *et al.* (The CDMS-II Collaboration), Science, **327**, 1619 (2010), arXiv:0912.3592[astro-ph.CO] .
[7] Z. Ahmed *et al.* (CDMS-II Collaboration), Phys.Rev.Lett., **106**, 131302 (2011), arXiv:1011.2482[astro-ph.CO] .
[8] E. Aprile *et al.* (XENON100 Collaboration), Phys.Rev.Lett. (2011), arXiv:1104.2549[astro-ph.CO] .
[9] J. Collar, (2011), arXiv:1103.3481[astro-ph.CO] .
[10] J. Collar, (2011), arXiv:1106.0653[astro-ph.CO] .
[11] M. T. Frandsen, F. Kahlhoefer, J. March-Russell, C. McCabe, M. McCullough, *et al.*, Phys.Rev., **D84**, 041301 (2011), arXiv:1105.3734[hep-ph] .
[12] P. J. Fox, J. Kopp, M. Lisanti, and N. Weiner, Phys.Rev., **D85**, 036008 (2012), arXiv:1107.0717[hep-ph] .
[13] M. Farina, D. Pappadopulo, A. Strumia, and T. Volansky, JCAP, **1111**, 010 (2011), arXiv:1107.0715[hep-ph] .
[14] T. Schwetz and J. Zupan, JCAP, **1108**, 008 (2011), arXiv:1106.6241[hep-ph] .
[15] C. McCabe, Phys.Rev., **D84**, 043525 (2011), arXiv:1107.0741[hep-ph] .
[16] J. Kopp, T. Schwetz, and J. Zupan, JCAP, **1203**, 001 (2012), arXiv:1110.2721[hep-ph] .
[17] D. Hooper and C. Kelso, Phys.Rev., **D84**, 083001 (2011), arXiv:1106.1066[hep-ph] .
[18] P. Belli, R. Bernabei, A. Bottino, F. Cappella, R. Cerulli, *et al.*, Phys.Rev., **D84**, 055014 (2011), arXiv:1106.4667[hep-ph] .
[19] C. Kelso, D. Hooper, and M. R. Buckley, Phys.Rev., **D85**, 043515 (2012), arXiv:1110.5338[astro-ph.CO] .
[20] M. T. Frandsen, F. Kahlhoefer, C. McCabe, S. Sarkar, and K. Schmidt-Hoberg, JCAP, **1201**, 024 (2012), arXiv:1111.0292[hep-ph] .
[21] O. Adriani *et al.* (PAMELA Collaboration), Nature, **458**, 607 (2009), arXiv:0810.4995[astro-ph] .
[22] A. A. Abdo *et al.* (The Fermi LAT Collaboration), Phys.Rev.Lett., **102**, 181101 (2009), arXiv:0905.0025[astro-ph.HE] .
[23] L. Bergstrom, J. Edsjo, and G. Zaharijas, Phys.Rev.Lett., **103**, 031103 (2009), arXiv:0905.0333[astro-ph.HE] .
[24] S. Desai *et al.* (Super-Kamiokande), Phys. Rev., **D70**, 083523 (2004), arXiv:hep-ex/0404025 .
[25] T. Tanaka *et al.* (Super-Kamiokande Collaboration), Astrophys.J., **742**, 78 (2011), arXiv:1108.3384[astro-ph.HE] .
[26] R. Abbasi *et al.* (ICECUBE), Phys. Rev. Lett., **102**, 201302 (2009), arXiv:0902.2460[astro-ph.CO] .
[27] I. Collaboration (IceCube Collaboration), (2011), arXiv:1112.1840[astro-ph.HE] .
[28] A. Aguilar *et al.* (LSND), Phys. Rev., **D64**, 112007 (2001), hep-ex/0104049 .
[29] A. A. Aguilar-Arevalo *et al.* (MiniBooNE), Phys. Rev. Lett., **105**, 181801 (2010), arXiv:1007.1150[hep-ex] .
[30] T. Mueller, D. Lhuillier, M. Fallot, A. Letourneau, S. Cormon, *et al.*, Phys.Rev., **C83**, 054615 (2011), arXiv:1101.2663[hep-ex] .
[31] G. Mention, M. Fechner, T. Lasserre, T. Mueller, D. Lhuillier, *et al.*, Phys.Rev., **D83**, 073006 (2011), arXiv:1101.2755[hep-ex] .
[32] P. Huber, Phys.Rev., **C84**, 024617 (2011), arXiv:1106.0687[hep-ph] .
[33] J. Kopp, M. Maltoni, and T. Schwetz, Phys.Rev.Lett., **107**, 091801 (2011), arXiv:1103.4570[hep-ph] .
[34] C. Giunti and M. Laveder, Phys.Rev., **D84**, 073008 (2011), arXiv:1107.1452[hep-ph] .
[35] C. Giunti and M. Laveder, Phys.Rev., **D84**, 093006 (2011), arXiv:1109.4033[hep-ph] .
[36] K. Abazajian, M. Acero, S. Agarwalla, A. Aguilar-Arevalo, C. Albright, *et al.*, (2012), arXiv:1204.

5379[hep-ph] .
[37] H. Nunokawa, O. Peres, and R. Zukanovich Funchal, Phys.Lett., **B562**, 279 (2003), arXiv:hep-ph/0302039[hep-ph] .
[38] S. Razzaque and A. Smirnov, JHEP, **1107**, 084 (2011), arXiv:1104.1390[hep-ph] .
[39] F. Halzen, (2011), arXiv:1111.0918[hep-ph] .
[40] V. Barger, Y. Gao, and D. Marfatia, Phys.Rev., **D85**, 011302 (2012), arXiv:1109.5748[hep-ph] .
[41] S. Razzaque and A. Y. Smirnov, (2012), arXiv:1203.5406[hep-ph] .
[42] J. N. Bahcall, A. M. Serenelli, and S. Basu, Astrophys.J., **621**, L85 (2005), Solar model data available from http://www.sns.ias.edu/∼jnb/, arXiv:astro-ph/0412440[astro-ph] .
[43] S. P. Mikheyev and A. Y. Smirnov, Sov. J. Nucl. Phys., **42**, 913 (1985).
[44] S. P. Mikheyev and A. Y. Smirnov, Nuovo Cim., **C9**, 17 (1986).
[45] L. Wolfenstein, Phys. Rev., **D17**, 2369 (1978).
[46] E. K. Akhmedov, , 103 (1999), arXiv:hep-ph/0001264[hep-ph] .
[47] T. Schwetz, M. Tortola, and J. Valle, New J.Phys., **13**, 109401 (2011), arXiv:1108.1376[hep-ph] .
[48] T. Schwetz, M. Tortola, and J. Valle, New J.Phys., **13**, 063004 (2011), arXiv:1103.0734[hep-ph] .
[49] A. E. Nelson and J. Walsh, Phys.Rev., **D77**, 033001 (2008), arXiv:arXiv:0711.1363[hep-ph] .
[50] J. Hamann, S. Hannestad, G. G. Raffelt, I. Tamborra, and Y. Y. Wong, Phys.Rev.Lett., **105**, 181301 (2010), arXiv:1006.5276[hep-ph] .
[51] E. Giusarma, M. Corsi, M. Archidiacono, R. de Putter, A. Melchiorri, *et al.*, Phys.Rev., **D83**, 115023 (2011), arXiv:1102.4774[astro-ph.CO] .
[52] J. Hamann, S. Hannestad, G. G. Raffelt, and Y. Y. Wong, JCAP, **1109**, 034 (2011), arXiv:1108.4136[astro-ph.CO] .
[53] E. Giusarma, M. Archidiacono, R. de Putter, A. Melchiorri, and O. Mena, Phys.Rev., **D85**, 083522 (2012), arXiv:1112.4661[astro-ph.CO] .
[54] G. Gelmini, S. Palomares-Ruiz, and S. Pascoli, Phys.Rev.Lett., **93**, 081302 (2004), arXiv:astro-ph/0403323[astro-ph] .
[55] A. Y. Smirnov and R. Zukanovich Funchal, Phys.Rev., **D74**, 013001 (2006), arXiv:hep-ph/0603009[hep-ph] .
[56] A. Gould, Astrophys. J. , **388**, 338 (1992).
[57] M. Blennow, J. Edsjo, and T. Ohlsson, (2007), http://www.physto.se/∼edsjo/wimpsim/.
[58] M. Blennow, J. Edsjo, and T. Ohlsson, JCAP, **0801**, 021 (2008), arXiv:0709.3898[hep-ph] .
[59] S. Jadach, Z. Was, R. Decker, and J. H. Kuhn, Comput.Phys.Commun., **76**, 361 (1993).
[60] M. Galassi *et al.*, *GNU Scientific Library Reference Manual*, 2nd ed. (Network Theory Ltd., 2003) ISBN 0-9541-617-34, http://www.gnu.org/software/gsl/.
[61] The IceCube Collaboration, (2011), arXiv:1111.2738[astro-ph.HE] .
[62] C. Arguelles, M. Bustamante, and A. Gago, JCAP, **1012**, 005 (2010), arXiv:1008.1396[astro-ph.HE] .
[63] H. B. Koers and P. Tinyakov, Phys.Rev., **D78**, 083009 (2008), arXiv:0802.2403[astro-ph] .
[64] R. Gandhi, C. Quigg, M. H. Reno, and I. Sarcevic, Phys.Rev., **D58**, 093009 (1998), arXiv:hep-ph/9807264[hep-ph] .
[65] M. Cirelli *et al.*, Nucl. Phys., **B727**, 99 (2005), arXiv:hep-ph/0506298 .
[66] C. Giunti and Y. Li, Phys.Rev., **D80**, 113007 (2009), arXiv:0910.5856[hep-ph] .
[67] H. S. Lee *et al.* (KIMS), Phys. Rev. Lett., **99**, 091301 (2007), arXiv:0704.0423[astro-ph] .
[68] E. Behnke, J. Behnke, S. Brice, D. Broemmelsiek, J. Collar, *et al.*, Phys.Rev.Lett., **106**, 021303 (2011), the updated results reproduced here were presented at TAUPP 2011, see http://taup2011.mpp.mpg.de/, arXiv:1008.3518[astro-ph.CO] .
[69] M. Felizardo, T. Girard, T. Morlat, A. Fernandes, F. Giuliani, *et al.*, (2011), arXiv:1106.3014[astro-ph.CO] .
[70] A. Esmaili and O. L. Peres, (2012), arXiv:1202.2869[hep-ph] .
[71] J. Stoer *et al.*, *Introduction to Numerical Analysis*, 3rd ed. (Springer, 2002) ISBN 038795452X.